

RESEARCH ARTICLE | APRIL 19 2023

# High-Q guided-mode resonance of a crossed grating with near-flat dispersion

Reuben Amedalor; Petri Karvinen; Henri Pesonen; ... et. al



*Appl. Phys. Lett.* 122, 161102 (2023)

<https://doi.org/10.1063/5.0138666>



CrossMark

## Articles You May Be Interested In

Space-Variant Model Fitting and Selection for Image Information Extraction

*AIP Conference Proceedings* (November 2006)

Simplified methods for the evaluation of seismic performances of steel frames

*AIP Conference Proceedings* (April 2022)

Fabrication of a graded-wavelength guided-mode resonance filter photonic crystal

*Appl. Phys. Lett.* (September 2006)

**Time to get excited.**  
Lock-in Amplifiers – from DC to 8.5 GHz

[Find out more](#)

# High-Q guided-mode resonance of a crossed grating with near-flat dispersion

Cite as: Appl. Phys. Lett. **122**, 161102 (2023); doi: [10.1063/5.0138666](https://doi.org/10.1063/5.0138666)

Submitted: 13 December 2022 · Accepted: 31 March 2023 ·

Published Online: 19 April 2023









View Online



Export Citation



CrossMark

Reuben Amedalor,<sup>1,2</sup>  Petri Karvinen,<sup>2</sup>  Henri Pesonen,<sup>2,a)</sup>  Jari Turunen,<sup>2</sup>  Tapio Niemi,<sup>1</sup>  and Subhajit Bej<sup>1,a),b)</sup> 

## AFFILIATIONS

<sup>1</sup>Photonics Laboratory, Tampere University, FI-33720 Tampere, Finland

<sup>2</sup>Center for Photonics Sciences, University of Eastern Finland, FI-80101 Joensuu, Finland

<sup>a)</sup>Present address: Dispelix Oy, Metsänneidonkuja 10, 02130 Espoo, Finland

<sup>b)</sup>Author to whom correspondence should be addressed: [subhajit.bej@tuni.fi](mailto:subhajit.bej@tuni.fi)

## ABSTRACT

Guided-mode resonances in diffraction gratings are manifested as peaks (dips) in reflection (transmission) spectra. Resonances with smaller line widths, i.e., with higher Q-factors, ensure stronger light–matter interactions and are beneficial for field-dependent physical processes. However, these high-Q resonances often suffer from strong angular and spectral dispersions. We demonstrate that a class of resonant modes with extraordinarily weak dispersion and Q-factor  $\sim 1000$  can be excited in crossed gratings simultaneously with the modes with well-known linear dispersion. Furthermore, the polarization of the incoming light can be adjusted to engineer the dispersion of these modes, and strong to near-flat dispersion or vice versa can be achieved by switching between two mutually orthogonal linear polarization states. We introduce a semi-analytical model to explain the underlying physics behind these observations and perform full-wave numerical simulations and experiments to support our theoretical conjecture. The results presented here will benefit all applications that rely on resonances in free-space-coupled geometries.

© 2023 Author(s). All article content, except where otherwise noted, is licensed under a Creative Commons Attribution (CC BY) license (<http://creativecommons.org/licenses/by/4.0/>). <https://doi.org/10.1063/5.0138666>

Resonance anomalies of diffraction gratings have attracted wide attention for over half a century.<sup>1</sup> At first, metallic gratings were shown to have sharp reflection dips associated with the excitation of surface modes, now known as surface plasmon polaritons.<sup>2</sup> A different class of anomalies associated with guided-wave excitation in dielectric gratings has also been well studied.<sup>3</sup> The gratings that exhibit this type of anomaly manifested as sharp peaks in reflection, and corresponding dips in transmission spectra, are known as resonant waveguide gratings (RWGs) or guided-mode resonance filters (GMRFs). The character and the spectral shape of the anomaly depend critically on the structural geometry as well as on the arrival angle and the polarization state of the incident electromagnetic wave.

One of the most common geometries of a GMRF includes a linear binary grating on top of a thin-film optical waveguide, and resonance anomalies can be connected with the excitation of waveguide modes.<sup>4</sup> Diffraction from the grating enables phase matching of incident light with the propagating waveguide modes, which eventually radiate into free space and interfere with light in direct reflection and transmission (in zeroth diffraction order). Consequently, sharp peaks in reflection and dips in transmission are observed. GMRFs have been exploited for numerous applications, such as filtering and beam

splitting,<sup>5–8</sup> refractive index sensing,<sup>9,10</sup> optical signal processing,<sup>11</sup> diffractive identification,<sup>12</sup> and wavelength division multiplexing.<sup>13,14</sup>

GMRFs, with one-dimensional (1D) periodicity, have been studied the most. The nature of diffraction from 1D GMRFs depends on their illumination conditions. When the grating lines are perpendicular to the plane of incidence (POI), i.e., the plane containing the propagation vector of the incident harmonic wave and the unit vector normal to the grating surface, the propagation vectors of the diffracted waves lie in the POI. This excitation geometry is known as classical diffraction mounting. Whereas for conical diffraction mounting,<sup>15</sup> the grating lines form an arbitrary angle with the POI, and the diffracted wave vectors reside on the surface of a cone. The grating lines can also be parallel to the POI, and the situation is known as full-conical diffraction mounting. There are plenty of published works on the classical<sup>16,17</sup> and conical diffraction mounting geometries of 1D GMRFs.<sup>18,19</sup>

One crucial characteristic of a GMRF is its resonance linewidth, which is often defined in terms of the Q-factor, defined as the ratio of the resonance peak wavelength to the resonance linewidth and usually scales inversely with the angular bandwidth of the incident light beam. Lemarchand *et al.* proposed using a grating with two collinear

periodicities to maintain high-Q and wider angular tolerance simultaneously.<sup>20</sup> Larger angular acceptance could also be obtained under a full-conical diffraction mounting of a 1D GMRF.<sup>21</sup>

Two-dimensional (2D) GMRFs, i.e., gratings with two noncollinear, in-plane lattice periodicities, are also extensively studied. One particular case of a 2D grating is a crossed grating where the two grating lines are orthogonal to each other. Peng and Morris theoretically investigated the guided mode resonances in a crossed grating<sup>22</sup> and later experimentally demonstrated the resonant modes at normal incidence of light.<sup>23</sup> Mizutani *et al.* realized polarization independence using a 2D grating with a rhombic lattice structure.<sup>24</sup> Fehrembach *et al.* developed a phenomenological theory for 2D GMRFs.<sup>25</sup> Later, they introduced a perturbative approach to analyze the resonant modes at an oblique incidence.<sup>26</sup> Wang *et al.* attempted to explain the origin of various spectral features of 2D GMRFs with rectangular lattices<sup>27</sup> and proposed design principles for polarization-independent 2D GMRFs for non-normal incidence of a plane wave.<sup>28</sup> Magnusson *et al.* studied the angular tunability of the resonances supported by a 2D GMRF experimentally in the long-wave infrared (night-vision) spectral band and explained their results using an effective medium approach of equivalent 1D gratings.<sup>29</sup>

In this Letter, we experimentally demonstrate that in a 2D grating, a type of high-Q resonance with near-flat dispersion can be excited with the typical dispersive resonant mode. Additionally, we show that the polarization state of light can control the dispersion characteristics of the resonances. Specifically, by switching between two mutually orthogonal linear polarization states, one can trigger a change from linear to near-zero dispersion. We perform full-wave numerical simulations to match the experimental results and use a semi-analytical approach based on the waveguide theory to provide clear physical insights behind the observations.

The geometry of our GMRF is depicted in Fig. 1, which consists of a 2D periodic surface-relief binary grating on top of a thin waveguiding layer. The incident and substrate regions are homogeneous

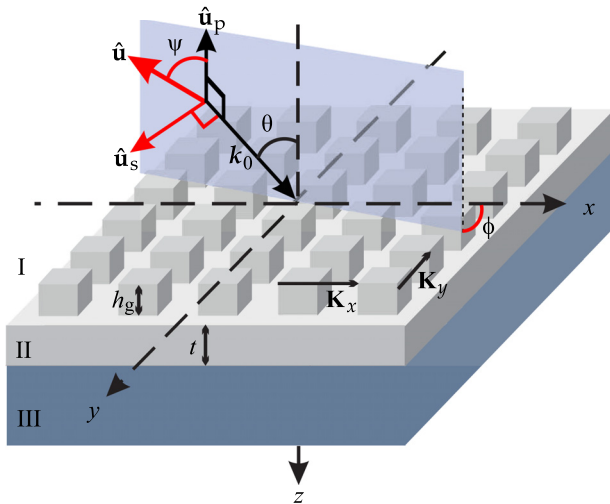


**FIG. 1.** Schematic of a square-lattice GMRF with periodicities along  $x$  and  $y$  under conical illumination. The incident harmonic wave is linearly polarized with the electric field pointing along  $\hat{\mathbf{u}}$ . The POI is highlighted in blue color.  $\hat{\mathbf{u}}_s$  and  $\hat{\mathbf{u}}_p$  are the components of  $\hat{\mathbf{u}}$  perpendicular and parallel to the POI, respectively.

media with refractive indices  $n_i$  (air) and  $n_s$  (fused silica), respectively. The grating and the waveguide are made of the same silicon nitride ( $\text{SiN}_x$ ) material with refractive index  $n_g$ . Grating periodicities along  $x$ - and  $y$ -axes are  $\Lambda_x$  and  $\Lambda_y$ , and the grating line widths are  $f_x\Lambda_x$  and  $f_y\Lambda_y$ , respectively. A linearly polarized harmonic wave with wave number  $k_0$  is incident from the air at an angle of incidence (AOI)  $\theta$  with  $z$ -axis. The angle  $\phi$  between the POI and the  $x$ -axis is the conical angle of incidence. Unit vector characterizing polarization is denoted by  $\hat{\mathbf{u}}$ , and  $\psi$  is the polarization angle. For the conical incidence of any plane wave, the wave vector  $\mathbf{k}_0$  can be written as

$$\mathbf{k}_0 = k_{x0}\hat{\mathbf{x}} + k_{y0}\hat{\mathbf{y}} + k_{z0}\hat{\mathbf{z}} = k_0(\sin\theta\cos\phi\hat{\mathbf{x}} + \sin\theta\sin\phi\hat{\mathbf{y}} + \cos\theta\hat{\mathbf{z}}). \quad (1)$$

Upon incidence on the GMRF, the plane wave gets diffracted, and the wave vectors of the diffracted light can be expressed as

$$\mathbf{k}_{q,mn} = k_{xm}\hat{\mathbf{x}} + k_{yn}\hat{\mathbf{y}} + k_{zq,mn}\hat{\mathbf{z}} = (k_{x0} + mK_x)\hat{\mathbf{x}} + (k_{y0} + nK_y)\hat{\mathbf{y}} + \sqrt{(k_q^2 - k_{xm}^2 - k_{yn}^2)}\hat{\mathbf{z}}, \quad (2)$$

where  $q = 1$  and  $3$  stand for regions I and III (the superstrate and the substrate as illustrated in Fig. 1), respectively, and  $m$  and  $n$  are integers representing the diffraction orders along  $x$  and  $y$ -axes, respectively. The grating vectors are  $\mathbf{K}_x = (2\pi/\Lambda_x)\hat{\mathbf{x}}$  and  $\mathbf{K}_y = (2\pi/\Lambda_y)\hat{\mathbf{y}}$ .

For a high-Q GMRF, the fields remain tightly confined inside the waveguide layer. Therefore, one can use the theory of an unperturbed slab waveguide to estimate the spectral peak positions of the resonances accurately. We use a multilayer waveguide mode solver<sup>30</sup> to evaluate the effective refractive indices  $n_{\text{eff}}$  of the modes in the  $\text{SiN}_x$  slab waveguide layer. Effective indices of the modes are plotted against the thickness ( $t$ ) of the waveguide in Fig. 2(a). The plots show that the thickness of the waveguide layer limits the maximum number of supported modes. These modes can be classified either as TE, where  $\mathbf{E}$ -field, or TM, where  $\mathbf{H}$ -field are perpendicular to the directions of propagation of the modes. We chose a waveguide layer thickness of  $t = 0.245\ \mu\text{m}$  [violet vertical dashed line in Fig. 2(a)] for the experimental demonstration. Clearly, this waveguide thickness can support one  $\text{TE}_0$  (fundamental TE) mode and one  $\text{TM}_0$  (fundamental TM) mode with effective mode indices  $n_{\text{eff}}^{\text{TE}_0} = 1.7381$  and  $n_{\text{eff}}^{\text{TM}_0} = 1.6269$ , respectively. The propagation constant  $\beta$  of the supported waveguide modes is defined as  $\beta = n_{\text{eff}}k_0$ .

The resonance anomalies are observed when the grating diffraction matches the tangential wave number of the incident wave with the propagation constant of a slab waveguide mode. This condition, also known as the phase-matching condition, can, in general, be written as

$$|k_{xm}\hat{\mathbf{x}} + k_{yn}\hat{\mathbf{y}}| = \beta = n_{\text{eff}}k_0. \quad (3)$$

Using Eqs. (1) and (2), it can be rewritten in the following form:

$$\left(k_0\sin\theta\cos\phi + \frac{2\pi m}{\Lambda_x}\right)^2 + \left(k_0\sin\theta\sin\phi + \frac{2\pi n}{\Lambda_y}\right)^2 = \beta^2. \quad (4)$$

We first analyze the normal incidence scenario with the  $xz$ -plane as the POI ( $\theta = 0^\circ$  and  $\phi = 0^\circ$ ). For  $s$ -polarization, the  $\mathbf{E}$ -field is

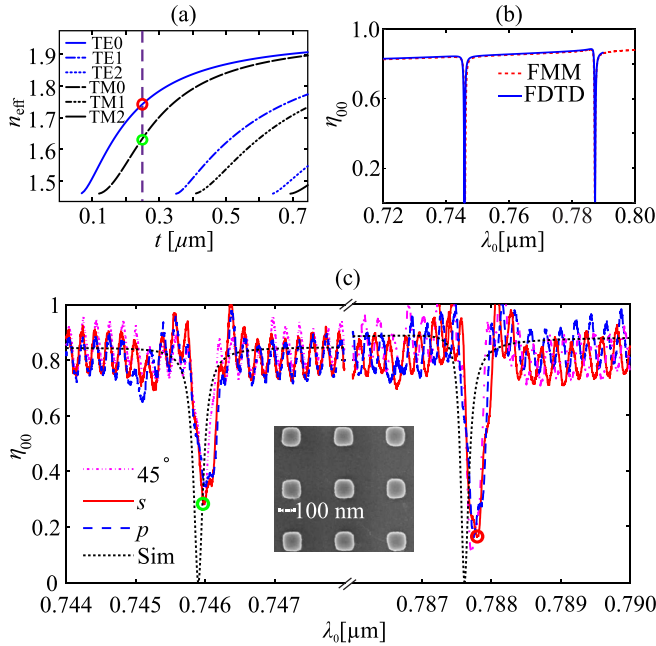


**FIG. 2.** (a) Effective indices ( $n_{\text{eff}}$ ) of the modes vs waveguide thickness  $t$ .<sup>30</sup> The wavelength (in the air) of the incident harmonic wave is  $\lambda_0 = 0.744 \mu\text{m}$ , and  $n_s = 1.46$  and  $n_g = 1.95$  are used in the calculations. (b) Diffraction efficiency in transmission calculated with the FMM and the FDTD-based solvers for  $s$ ,  $p$ , or  $45^\circ$  polarized harmonic wave in normal incidence from the air.  $\Lambda_x = \Lambda_y = 0.451 \mu\text{m}$ ,  $f_x = f_y = 0.46$ ,  $h_0 = 0.045 \mu\text{m}$ , and  $t = 0.245 \mu\text{m}$  are used in the numerical simulations. (c) Comparison of diffraction efficiency in direct transmission obtained experimentally for normal incidence of  $s$ ,  $p$ , and  $45^\circ$  linearly polarized light with numerical simulations (black dotted lines). The inset shows a scanning electron microscope image (top-view) of the fabricated GMRF.

parallel to  $y$ -axis, and the projection of  $\mathbf{k}_0$  on the  $xy$ -plane is parallel with  $x$ -axis. For a better understanding, we can think of this complete diffraction problem as a combination of diffraction from two 1D gratings (one grating with periodicity along the  $x$ -axis and another with periodicity along the  $y$ -axis). Hence, the grating periodic along the  $x$ -axis is under classical diffraction mounting for  $s$ -polarized light incidence. At the same time, the  $y$ -periodic grating is under full-conical illumination. For normal incidence, Eq. (4) reduces to

$$\sqrt{\left(\frac{2\pi m}{\Lambda_x}\right)^2 + \left(\frac{2\pi n}{\Lambda_y}\right)^2} = \pm \frac{2\pi}{\lambda_0} n_{\text{eff}}^{\text{TE/TM}}. \quad (5)$$

The diffraction orders  $(m, n) = (\pm 1, 0)$  excite the  $\text{TE}_0$  waveguide modes propagating along  $\pm x$ -directions, and the spectral peak position of the resonance ( $\Gamma$ -point) is at  $\lambda_0^{\text{TE}_0} = 0.788 \mu\text{m}$ , which is obtained by using  $n_{\text{eff}}^{\text{TE}_0} = 1.7381$  in Eq. (5). Simultaneously, the  $(0, \pm 1)$  diffraction orders excite the  $\text{TM}_0$  waveguide modes at  $\lambda_0^{\text{TM}_0} = 0.744 \mu\text{m}$  (F-point) propagating along  $\pm y$ -directions.

To validate the preceding analytical predictions of the spectral positions of the resonances, we perform full-wave numerical simulations with in-house software based on the well-known Fourier Modal Method (FMM).<sup>31</sup> The FMM-based simulation results are also compared with Finite-Difference Time-Domain (FDTD) simulations based

on a commercial solver.<sup>32</sup> For both methods, careful convergence tests are performed to ensure the accuracy of the numerical results (see Sec. 1 of the [supplementary material](#)). Furthermore, an experimentally measured refractive index data of  $\text{SiN}_x$  is used in the numerical (FMM and FDTD) simulations (see Sec. 2 of the [supplementary material](#)). The transmittance spectrum for illumination with a  $s$ -polarized harmonic wave is shown in Fig. 2(b). For normal incidence, the spectrum is polarization-independent. Hence, one can obtain identical simulation results with  $s$ ,  $p$ , and  $45^\circ$  linear polarizations.

For experimental demonstration, a square-lattice GMRF with the designed grating parameters is fabricated with standard lithographic processes, which include steps such as chemical vapor deposition, electron beam lithography, and reactive ion etching (see Sec. 3 of the [supplementary material](#) for the fabrication details). The transmission spectra of the GMRF are measured with a custom-built transmission setup. A supercontinuum light source is used, and the transmittance in zeroth diffraction order is measured with an optical spectrum analyzer (OSA). The GMRF is mounted on a 2-axis goniometer placed on top of a rotation stage to control both  $\theta$  and  $\phi$  (see Sec. S4 in the [supplementary material](#) for details of the experimental procedure). The normalized efficiency in direct transmission ( $\eta_{00}$ ) for  $s$ ,  $p$ , and  $45^\circ$  linear polarizations of light incident from the air with  $\theta = 0^\circ$  and  $\phi = 0^\circ$  is shown in Fig. 2(c). The plots obtained with FMM (identical for  $s$ ,  $p$ , and  $45^\circ$  linear polarizations) are also included for direct comparison with the experimental results. The difference in the spectral positions of the resonances obtained numerically and experimentally is due to the difference in grating periods/fill factors in the design and the fabricated structure. Also, the numerical results show higher Q-factors than those obtained experimentally, which can be attributed to fabrication imperfections and limitations of the measurement procedure. The Q-factors of the resonances estimated from the experimental plots in Fig. 2(c) are  $\approx 4500$ . Figures 2(a)–2(c) show that the analytical predictions, full-wave numerical simulations, and experimental results are in good agreement.

We calculate the field distributions inside the GMRF with the FDTD-based solver to confirm the analytical predictions of the mode propagation directions. Figure 3 shows the simulation results. The excitation wavelength is set as  $\Gamma_s = 0.7878 \mu\text{m}$  for the  $E$ -field plot in Fig. 3(a). For the  $H$ -field plot in Fig. 3(b), the excitation wavelength is  $F_s = 0.7457 \mu\text{m}$ . In both plots,  $s$ -polarized light is incident normally onto the GMRF from the air. The plots show that excitations of the guided modes result in strong confinements and enhancements of the fields within the waveguide. Moreover, the  $\text{TE}_0$  and the  $\text{TM}_0$  modes propagate along the  $x$ - and  $y$ -axes, respectively.

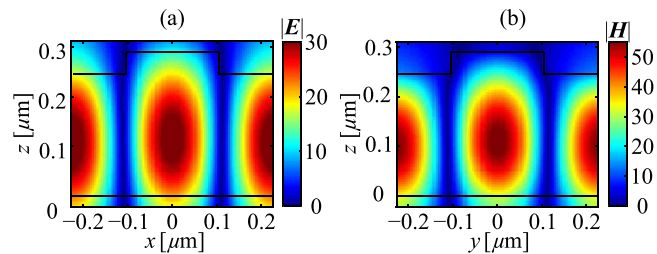


**FIG. 3.** Fields inside the GMRF at resonance. (a) The  $E$  field inside the GMRF normalized to the incident EM wave for  $\lambda_0 = \Gamma_s$ , and (b) the normalized  $H$  field inside the grating at  $\lambda_0 = F_s$ .

We proceed to investigate the angular and spectral dispersion characteristics of the resonances. For the oblique incidence of a harmonic wave ( $\theta \neq 0^\circ$ ) and for  $\phi = 0^\circ$ , Eq. (4) can either take the form of Eq. (6) or Eq. (7), which solely depends on the indices ( $m, n$ ) of the diffraction orders that excite the guided modes. For  $s$ -polarized light, the  $(m, n) = (\pm 1, 0)$  diffraction orders of the grating excite the  $TE_0$  waveguide modes propagating along  $\pm x$ -directions. Hence, the resonances related to the  $TE_0$  modes symmetrically split into two branches, as shown by the following equation:

$$\pm k_0 \sin \theta + \frac{2\pi m}{\Lambda_x} = \pm \frac{2\pi}{\lambda_0} n_{\text{eff}}^{\text{TE}}. \quad (6)$$

The resulting V-shaped dispersion is plotted in Fig. 4(a) as the dashed lines extending from  $\Gamma_s = 0.788 \mu\text{m}$ . Simultaneously, the  $(m, n) = (0, \pm 1)$  diffraction orders can excite both  $TM_0$  and  $TE_0$  waveguide modes. For these degenerate modes, Eq. (4) can be written as

$$\sqrt{(k_0 \sin \theta)^2 + \left(\frac{2\pi n}{\Lambda_y}\right)^2} = \pm \frac{2\pi}{\lambda_0} n_{\text{eff}}^{\text{TM/TE}}, \quad (7)$$

which shows no splitting of the nearly flat dispersion curve as illustrated with the dashed line originating from  $F_s = 0.744 \mu\text{m}$  (for the  $TM$  mode) in Fig. 4(a). It should be noted that the near-flat  $TE$  modes excited by the  $(m, n) = (0, \pm 1)$  diffraction orders propagate along  $k_x \hat{x} \pm K_y \hat{y}$ . For small values of  $\theta$ , the coupling of  $s$ -polarized light with these  $TE$ -modes is small due to the polarization symmetry (see Sec. 5 in the supplementary material). At normal incidence, this coupling possibility vanishes completely, resulting in band gaps.

For  $p$  polarized light, the  $(m, n) = (\pm 1, 0)$  diffraction orders of the grating excite the  $TM_0$  guided modes resulting in the V-shaped dispersion curve starting from  $\Gamma_p$ . Simultaneously, both  $TM_0$  and  $TE_0$  modes are excited with the  $(m, n) = (0, \pm 1)$  diffraction orders displaying nearly flat dispersion characteristics as shown in Fig. 4(b).

Any arbitrary linear polarization state of light can be considered a sum of the  $s$  and  $p$  polarized components. For values of  $\psi$  other than  $0^\circ$  or  $90^\circ$ , both the  $(m, n) = (\pm 1, 0)$  and  $(m, n) = (0, \pm 1)$  diffraction orders of the grating can excite  $TE_0/TM_0$ -type slab waveguide

modes efficiently. The dashed lines in Fig. 4(c) show the angular/spectral dispersion of the modes for the oblique incidence of a  $45^\circ$  polarized harmonic wave. Four branches of the dispersion curves can be observed for  $\theta \neq 0^\circ$ . Two are V-shaped, whereas the other two are almost horizontal lines. Hence, the dispersion characteristics for  $45^\circ$  linear polarization case can be seen as a combination of the  $s$  and  $p$  polarized cases.

The numerically calculated transmission spectra with FMM are also included in Fig. 4. The color bar indicates the normalized transmittance ( $\eta_{00}$ ) in direct transmission. We notice that the  $\Gamma$  and the  $F$  points obtained with the two approaches agree very well. However, as  $\theta$  increases, the dispersion curves obtained with the analytical formulation start to deviate from those obtained with FMM. This difference can be attributed to wavelength-dependent mode indices. The analytical solution of the dispersion curve in Eq. (4) assumes a constant  $n_{\text{eff}}$ . However, a modified  $n_{\text{eff}}(\lambda_0)$  should be considered for a more accurate analytic estimation.

The experimentally measured peak wavelengths of the transmittance curves at discrete  $\theta$  are also included in Fig. 4. The red (green) and green (red) circle positions correspond to  $\Gamma$  and  $F$  points for  $s$  ( $p$ ) polarization. The experimentally obtained resonance peak positions  $\Gamma_s = 0.788 \mu\text{m}$  and  $F_s = 0.746 \mu\text{m}$  are in excellent agreement with the simulation results. The error bars along  $\lambda_0$  and  $\theta$  axes are related to the measurement uncertainties (see Sec. 6 of the supplementary material).

In summary, we have identified and experimentally verified a type of guided-mode resonance with ultra-low spectral and angular dispersion in a crossed grating. The dispersion index ( $\Delta\lambda_0/\Delta\theta$ ) of this resonance with Q-factor  $\approx 4500$  is  $\sim 10^{-5} \mu\text{m}/^\circ$ , which is about three orders of magnitude smaller than the dispersion of a typical guided-mode resonance with a similar Q-factor. In addition, we experimentally demonstrate that in a 2D grating, one can switch between conventional linear and near-flat dispersion of the resonances by switching from  $s$  to  $p$ -polarized light incidence and vice versa. The results presented in this Letter show that achieving high-Q and low dispersion simultaneously with a free-space diffractive optical element is possible and will benefit many practical applications in optoelectronics and photonics that rely on resonances from free-space-coupled geometries.

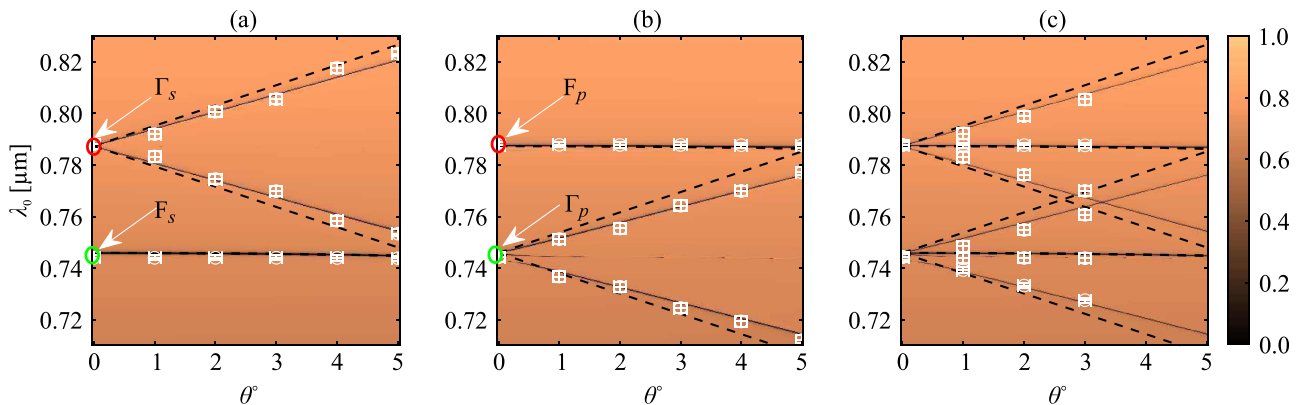


FIG. 4. Diffraction efficiency in direct transmission plotted against  $\lambda_0$  and  $\theta$  for (a)  $s$ -polarized ( $\psi = \pi/2$ ), (b)  $p$ -polarized ( $\psi = 0$ ), and (c)  $45^\circ$  linearly polarized illumination ( $\psi = \pi/4$ ). The continuous lines indicate the FMM solver-based numerical simulation results, the dispersion plots obtained with Eq. (4) are indicated with the dashed lines, and the white circles with error bars mark the experimental results. The color bar scaled from “0” to “1” indicates the transmittance value.

See the [supplementary material](#) for the supporting contents: 1. Numerical convergence test. 2. The refractive index of Silicon Nitride measured with ellipsometry. 3. Fabrication method in detail. 4. Detailed experimental procedure. 5. Explanations with k-space diagrams. 6. Details of measurement uncertainties.

The authors thank Timo Stolt and Alireza Rahimi Rashed for the helpful discussions during the planning stage of the optical measurements.

This work was supported by the Flagship of Photonics Research and Innovation (PREIN) funded by the Academy of Finland—Grant Nos. 31001498, 320165 (Tampere University), and 320166 (University of Eastern Finland).

## AUTHOR DECLARATIONS

### Conflict of Interest

The authors have no conflicts to disclose.

### Author Contributions

**Reuben Amedalor:** Formal analysis (lead); Investigation (equal); Methodology (equal); Software (equal); Validation (equal); Visualization (equal); Writing – original draft (equal); Writing – review & editing (equal). **Petri Karvinen:** Investigation (supporting); Methodology (supporting). **Henri Pesonen:** Investigation (supporting); Software (supporting). **Jari Turunen:** Funding acquisition (supporting); Supervision (equal); Writing – review & editing (supporting). **Tapio Kari Niemi:** Conceptualization (equal); Funding acquisition (lead); Investigation (supporting); Resources (equal); Supervision (equal); Writing – original draft (supporting); Writing – review & editing (supporting). **Subhajit Bej:** Conceptualization (equal); Formal analysis (supporting); Investigation (lead); Methodology (lead); Project administration (equal); Resources (equal); Software (equal); Supervision (equal); Validation (equal); Visualization (equal); Writing – original draft (lead); Writing – review & editing (lead).

### DATA AVAILABILITY

The data that support the findings of this study are available from the corresponding author upon reasonable request.

### REFERENCES

- R. Petit, *Electromagnetic Theory of Gratings* (Springer, Berlin, 1980).
- R. Wood, “XLII. On a remarkable case of uneven distribution of light in a diffraction grating spectrum,” *London, Edinburgh, Dublin Philos. Mag. J. Sci.* **4**, 396–402 (1902).
- G. Quaranta, G. Basset, O. J. F. Martin, and B. Gallinet, “Recent advances in resonant waveguide gratings,” *Laser Photonics Rev.* **12**, 1800017 (2018).
- S. S. Wang and R. Magnusson, “Theory and applications of guided-mode resonance filters,” *Appl. Opt.* **32**, 2606–2613 (1993).
- Z. S. Liu, S. Tibuleac, D. Shin, P. P. Young, and R. Magnusson, “High-efficiency guided-mode resonance filter,” *Opt. Lett.* **23**, 1556–1558 (1998).
- Y. Kanamori, N. Matsuyama, and K. Hane, “Resonant-wavelength tuning of a pitch-variable 1-D photonic crystal filter at telecom frequencies,” *IEEE Photonics Technol. Lett.* **20**, 1136–1138 (2008).
- M. Streshinsky, R. Shi, A. Novack, R. T. P. Cher, A. E.-J. Lim, P. G.-Q. Lo, T. Baehr-Jones, and M. Hochberg, “A compact bi-wavelength polarization splitting grating coupler fabricated in a 220 nm SOI platform,” *Opt. Express* **21**, 31019–31028 (2013).
- Y. Xu, X. Gao, D. Bai, G. Zhu, J. Yuan, H. Zhu, and Y. Wang, “Free-space-to-waveguide demultiplexer featuring zero-contrast gratings,” *Opt. Commun.* **387**, 89–94 (2017).
- H. Kikuta, N. Maegawa, A. Mizutani, K. Iwata, and H. Toyota, “Refractive index sensor with a guided-mode resonant grating filter,” in *Optical Engineering for Sensing and Nanotechnology (ICOSN 2001)*, edited by K. Iwata (SPIE, 2001), Vol. 4416, pp. 219–222.
- R. Magnusson, D. Wawro, S. Zimmerman, and Y. Ding, “Resonant photonic biosensors with polarization-based multiparametric discrimination in each channel,” *Sensors* **11**, 1476–1488 (2011).
- L. L. Doskolovich, D. A. Bykov, E. A. Bezus, and V. A. Soifer, “Spatial differentiation of optical beams using phase-shifted Bragg grating,” *Opt. Lett.* **39**, 1278–1281 (2014).
- M.-L. Wu, C.-L. Hsu, H.-C. Lan, H.-I. Huang, Y.-C. Liu, Z.-R. Tu, C.-C. Lee, J.-S. Lin, C.-C. Su, and J.-Y. Chang, “Authentication labels based on guided-mode resonant filters,” *Opt. Lett.* **32**, 1614–1616 (2007).
- K. Kintaka, K. Shimizu, Y. Kita, S. Kawanami, J. Inoue, S. Ura, and J. Nishii, “Potential characterization of free-space-wave drop demultiplexer using cavity-resonator-integrated grating input/output coupler,” *Opt. Express* **18**, 25108–25115 (2010).
- R. Magnusson, “Spectrally dense comb-like filters fashioned with thick guided-mode resonant gratings,” *Opt. Lett.* **37**, 3792–3794 (2012).
- M. G. Moharam, E. B. Grann, D. A. Pommet, and T. K. Gaylord, “Formulation for stable and efficient implementation of the rigorous coupled-wave analysis of binary gratings,” *J. Opt. Soc. Am. A* **12**, 1068–1076 (1995).
- D. Rosenblatt, A. Sharon, and A. Friesem, “Resonant grating waveguide structures,” *IEEE J. Quantum Electron.* **33**, 2038–2059 (1997).
- M. R. Saleem, D. Zheng, B. Bai, P. Stenberg, M. Kuittinen, S. Honkanen, and J. Turunen, “Replicable one-dimensional non-polarizing guided mode resonance gratings under normal incidence,” *Opt. Express* **20**, 16974–16980 (2012).
- D. Lacour, G. Granet, J.-P. Plumey, and A. Mure-Ravaud, “Polarization independence of a one-dimensional grating in conical mounting,” *J. Opt. Soc. Am. A* **20**, 1546–1552 (2003).
- G. Niederer, W. Nakagawa, H. P. Herzig, and H. Thiele, “Design and characterization of a tunable polarization-independent resonant grating filter,” *Opt. Express* **13**, 2196–2200 (2005).
- F. Lemarchand, A. Sentenac, and H. Giovannini, “Increasing the angular tolerance of resonant grating filters with doubly periodic structures,” *Opt. Lett.* **23**, 1149–1151 (1998).
- Y. H. Ko, M. Niraula, and R. Magnusson, “Divergence-tolerant resonant band-pass filters,” *Opt. Lett.* **41**, 3305–3308 (2016).
- S. Peng and G. M. Morris, “Resonant scattering from two-dimensional gratings,” *J. Opt. Soc. Am. A* **13**, 993–1005 (1996).
- S. Peng and G. M. Morris, “Experimental demonstration of resonant anomalies in diffraction from two-dimensional gratings,” *Opt. Lett.* **21**, 549–551 (1996).
- A. Mizutani, H. Kikuta, K. Nakajima, and K. Iwata, “Nonpolarizing guided-mode resonant grating filter for oblique incidence,” *J. Opt. Soc. Am. A* **18**, 1261–1266 (2001).
- A.-L. Fehrembach, D. Maystre, and A. Sentenac, “Phenomenological theory of filtering by resonant dielectric gratings,” *J. Opt. Soc. Am. A* **19**, 1136–1144 (2002).
- A.-L. Fehrembach and A. Sentenac, “Study of waveguide grating eigenmodes for unpolarized filtering applications,” *J. Opt. Soc. Am. A* **20**, 481–488 (2003).
- D. Wang and Q. Wang, “Spectral features of guided mode resonant filter with two-dimensional crossed grating,” *J. Lightwave Technol.* **37**, 4445–4450 (2019).
- D. Wang, Q. Wang, and Z. Zhan, “Polarization-independent filter based on 2-D crossed grating under oblique incidence,” *IEEE Photonics J.* **10**, 1–9 (2018).
- Y. H. Ko, K. J. Lee, F. A. Simlan, N. Gupta, and R. Magnusson, “Dual angular tunability of 2D Ge/ZnSe notch filters: Analysis, experiments, physics,” *Adv. Opt. Mater.* **11**, 2202390 (2023).
- M. Hammer, see <https://www.sio.eu/oms.html> for “1-D mode solver for dielectric multilayer slab waveguides” (2022).
- L. Li, “New formulation of the Fourier modal method for crossed surface-relief gratings,” *J. Opt. Soc. Am. A* **14**, 2758–2767 (1997).
- See <https://www.lumerical.com/products/fdtd/> for “FDTD: 3D electromagnetic simulator” (2022).